A System for Measuring the Characteristics of High Peak Power Detectors of Pulsed CO_2 Radiation

Philip A. Simpson

Electromagnetic Technology Division
National Engineering Laboratory
National Bureau of Standards
Boulder, Colorado 80303

U.S. DEPARTMENT OF COMMERCE, Philip M. Klutznick, Secretary

Luther H. Hodges, Jr., Deputy Secretary
Jordan J. Baruch, Assistant Secretary for Productivity, Technology and Innovation

NATIONAL BUREAU OF STANDARDS, Ernest Ambler, Director

Issued September 1980

NATIONAL BUREAU OF STANDARDS TECHNICAL NOTE 1023

Nat. Bur. Stand. (U.S.), Tech. Note 1023, 48 pages (Sept. 1980)

CODEN: NBTNAE

U.S. GOVERNMENT PRINTING OFFICE
WASHINGTON: 1980

CONTENTS

List of Figures

A System for Measuring the Characteristics of High Peak Power Detectors of Pulsed CO_2 Radiation

Philip A. Simpson

A system is described for determining the responsivity of detectors for high peak power CO_2 laser pulses. The insertion loss of feed-through detectors can also be measured. The basic approach involves a measurement of the excitation energy and detector output waveform, and is applicable only for pulse amplitudes where the detector output voltage is a linear function of the optical power. However, a method is described for extending measurements to power levels where the responsivity becomes nonlinear. The time response of the detectors is checked using short duration (10 ns) rectangular pulses to simulate an impulse. A method for measuring beam diameter is also detailed. An error analysis of the system is given.

Key words: Beam diameter; insertion loss; optical detectors; photon drag detector; pyroelectric detector; responsivity; single longitudinal mode pulse; TEA laser.

1. Introduction

High peak power pulsed CO_2 laser radiation is finding increased use in today's high technology fields. Two of the more prominent programs that employ this type of radiation are the laser fusion [1] and laser rangefinder[1] programs. Pulses of this type are also a useful tool in property of materials studies [2] since they are capable of producing high values of energy and electric field in periods of less than 1 μs. The need for well characterized detectors for this type of radiation is therefore essential for attaining accurate measurement results in these fields.

The National Bureau of Standards Boulder Laboratories have recently developed a system for characterizing power measuring detectors of CO_2 TEA laser pulses with a 10 ns time resolution. The type of detectors measured with this system are room temperature operating ones, capable of measuring relatively high peak powers (> 100 kW) with little or no attenuation. These devices generally include such types as photon drag and pyroelectric detectors. However, the techniques and principles used in this system are readily adaptable to the characterization of low peak power detectors with modifications mainly to adjust the amplitude of the optical signal. Also the system can be extended to other wavelengths by the replacement of certain wavelength-sensitive elements.

---

[1]This work was supported by the Calibration Coordination Group of the Department of Defense, the Air Force Avionics Laboratory, and the Office of Naval Research.

2. The Measurement Process

2.1 Characteristics to be Measured

The parameter in which we are primarily interested is the responsivity. This quantity relates the output electrical signal from a detector to the activating optical power. It is defined as R, the proportionality factor, in the following expression

$$V(t) = R \int G(t-t')P(t')dt \qquad (1)$$

where

$V(t)$ = the time function of detector output voltage, in volts,
R = the responsivity in V/W,
$G(t-t')$ = the detector impulse response in Hz, and
$P(t')$ = the time function of optical power in watts.

Another parameter we shall measure is the insertion loss of feed-through type detectors. This quantity tells how much a beam is attenuated when passed through the device and is defined as the ratio of the input power (or energy) to the output power (or energy). We are also interested in the maximum irradiance to which the detector is subjected in order to avoid possibly inducing such unwanted effects as saturation or damage. Irradiance, sometimes referred to as power density, usually is expressed in units of watts per square centimeter.

In making these optical measurements it is imperative that we use a spatially well-characterized beam. We need to know the beam size and profile so that we can determine the peak irradiance and also the percent of the total incident beam being captured by the detector. The kind of beam employed in this system, unless otherwise noted, is a TEM_{00} Gaussian beam since the mathematics for this simple type of beam is straightforward. Its diameter is defined as the diameter of the beam where the intensity falls to $1/e^2$ that of the maximum.

One other characteristic we will measure is the detector time response. For purposes in this paper, this is defined as the minimum optical pulse transition time that will be faithfully reproduced within certain prescribed limits of error. Knowledge of the time response of the detector is required when measuring fast pulses to ensure the detector output response is not being degraded due to inability of the detector to respond to the optical signals.

2.2 Responsivity Measurements

For terminating type detectors the responsivity is determined by measuring the energy incident upon the detector and the voltage output waveform from the detector. The responsivity is then calculated by dividing the area under the voltage waveform by the energy. The incident energy is measured using a calibrated beam splitter and calorimeter as shown in figure 1, while the output voltage waveform is measured with a transient digitizer. Thus,

$$R_i = \frac{A_v}{BE_c} \qquad (2)$$

where

R_i = the input responsivity of the detector in V/W,
A_v = the area under the voltage waveform in V·S,
B = the beam splitter ratio defined as the transmitted power divided by the reflected power, and
E_c = the energy measured by the calorimeter in joules.

For feed-through type detectors the responsivity associated with the output is also measured using an arrangement as shown in figure 2. Here

$$R_o = \frac{A_v}{E_c} \qquad (3)$$

where

R_o = the output responsivity of the detector in V/W,
A_v = the same as in eq (1) above, and
E_c = the energy measured by the calorimeter in joules.

These relatively straightforward procedures can contain subtle sources of error. First it must be established that the optical detector is operating in a region where its voltage output is a linear function of the optical power. This can be ascertained by inserting attenuators in the laser beam ahead of the beam splitter and verifying that the responsivity remains constant for pulses of different peak powers.

Another possible source of error arises from the fact that the calorimeter and/or detector may not be capturing all of the energy in their respective beams. Their apertures may not be big enough to contain all the energy in the beam. Reflectance losses in the detector are not considered separately but are included as part of the responsivity measurement. For calorimeters with apertures of 25 mm or more, beam capture errors are rather easy to avoid. However, detectors having apertures with dimensions of 1 to 5 mm pose a problem. To be able to fully capture "all" (99.97%) of the energy of a TEM_{00} Gaussian beam, the detector aperture should have twice the diameter of the beam at the $1/e^2$ intensity

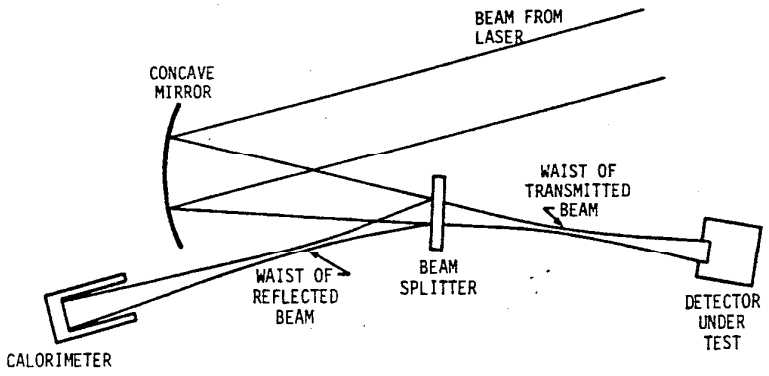

Figure 1. Arrangement of equipment for measuring the input responsivity of terminating type detectors.

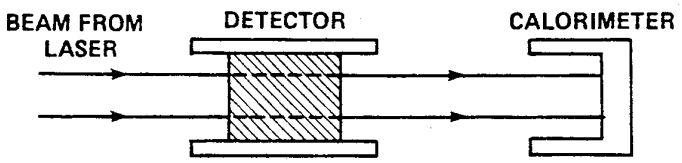

Figure 2. Arrangement of components for measuring the output responsivity of feed-through detectors.

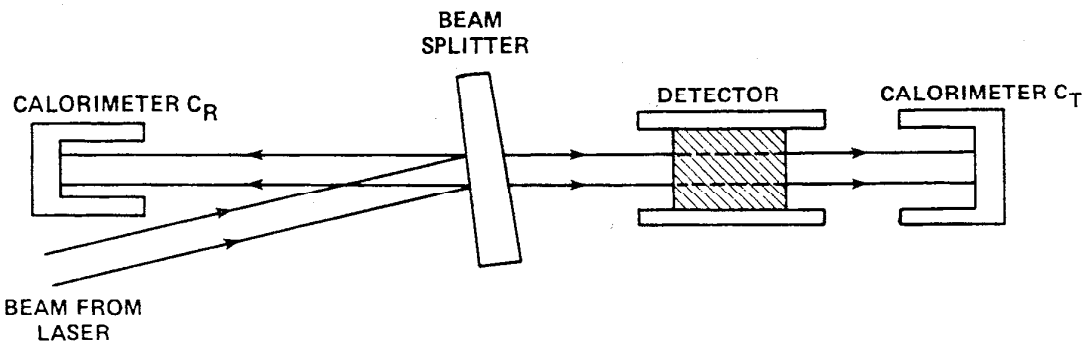

Figure 3. Arrangement of equipment for measuring insertion loss of feed-through detectors.

points. This means that some sort of focusing is usually required to reduce beam dimensions to the appropriate size.

Focusing results in increased irradiance. This fact may produce undesirable effects, such as nonlinear operation due to saturation or actual damage. The peak irradiance of a TEM_{00} beam is given by

$$P_o = \frac{2P_t}{\pi w^2} \tag{4}$$

where

P_o = the peak irradiance in W/cm^2,
P_t = the power in total beam in W,
w = the radius in cm of the beam at the $1/e^2$ intensity point.

Thus, remembering the stipulation of aperture diameter equal to twice the beam diameter, we find a 1 MW beam totally contained just within a circular area of 1 cm^2 (W=0.28 cm) has a peak irradiance of 8 MW/cm^2. If the beam is focused to fit totally within a 5 mm aperture the peak irradiance increases to 40 MW/cm^2 and for a 1 mm aperture the irradiance is 1 GW/cm^2. Obviously, these peak irradiances can cause problems.

2.3 Insertion Loss of Feed-Through Detectors

The insertion loss of feed-through detectors can be measured by several different methods. The most straightforward method involves measuring the input and output energies (powers) with a setup as in figure 3. We can say

$$\text{I.L.} = \frac{E_{in}}{E_{out}} = \frac{E_R B}{E_T} \tag{5}$$

where

I.L. = the insertion loss,
E_R = the energy measured by the calorimeter C_R,
B = the beam splitter ratio, and
E_T = the energy measured by the calorimeter C_T.

For linear devices it can also be shown that the insertion loss can be derived from a knowledge of the input and output responsivities as shown in eq (6) below

$$\text{I.L.} = \frac{R_o}{R_i} \tag{6}$$

where

R_o = the output responsivity in V/W, and

R_i = the input responsivity in V/W.

The insertion loss can also be determined with a tandem arrangement of feed-through detectors as shown in figure 4. The two detectors, "a" and "b", have previously had their R_o's determined. The energy is then measured with the calorimeter and the area under the waveform from detector "a" determined. We can then say

$$I.L._b = \frac{E_{ib}}{E_{ob}} . \tag{7}$$

Now

$$E_{ib} = \frac{V \cdot S_a}{R_{oa}} \tag{8}$$

where

$V \cdot S_a$ = area under the waveform from detector "a", and

R_{oa} = the output responsivity of detector "a" in V/W or V·S/J.

Also,

$$E_{ob} = J \tag{9}$$

where

J = the energy in joules measured by the calorimeter.

Substituting eqs (8) and (9) in eq (7) and simplifying yields

$$I.L. = \frac{V \cdot S_a}{J(R_{oa})} , \tag{10}$$

and if we define $V \cdot S_a/J = R'_{oa}$ as the "apparent" output responsivity of "a" with "b" inserted in the output beam, then

$$I.L_b = \frac{R'_{oa}}{R_{oa}} . \tag{11}$$

From a knowledge of the insertion loss and output responsivity the input responsivity can be determined from eq (6).

When using this tandem method for characterizing feed-through detectors it should be verified that reflections from detector "b" are low enough to cause negligible effect on the output waveform of detector "a". This is not an interference effect in photon drag detectors but is an actual subtraction to the output voltage caused by photons traveling in a direction opposite to the main beam [3].

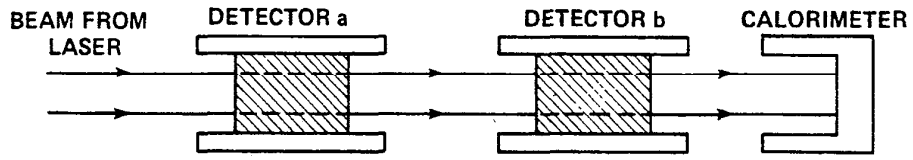

Figure 4. Tandem arrangement of feed-through detectors for measuring input and output responsivities and insertion loss.

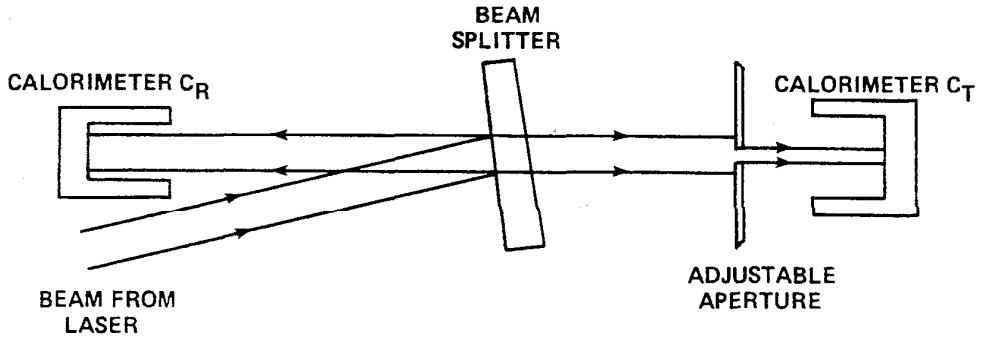

Figure 5. Arrangement of components for making beam diameter measurements.

2.4 Determination of Beam Diameter

Knowledge of the diameter of the TEM_{00} Gaussian beam is required for two purposes

a. calculation of the peak irradiance, and
b. verification that all of the energy is incident upon the surface of the detector or determination of the fraction of energy that is incident.

The procedure for measuring the diameter involves first adjusting the laser output mirror and an intercavity iris so that the laser produces a circular glowing spot on a carbon paddle [4]. This type of spot usually indicates the laser is operating in the TEM_{00} mode but it is possible to confuse this pattern with that produced by higher orders such as the TEM_{11}, TEM_{22}, etc. The construction details of some lasers may render it impossible to attain a TEM_{00} beam. In this case the size of the multimode beam should be determined by some other method, e.g., scanning.

To confirm that the mode structure is totally TEM_{00}, we insert an adjustable aperture in the beam and fix its diameter so it intercepts part of the energy in the periphery of the beam. Figure 5 shows an arrangement of components for making a beam diameter measurement. The transmittance of a circular aperture centered on a TEM_{00} Gaussian beam is given by

$$T = 1 - e^{\frac{-2a^2}{w^2}} \qquad (12)$$

where

T = the transmittance, i.e., the fraction of energy in the total beam transmitted through the aperture,
a = radius of aperture, and
w = radius of the total beam at the $1/e^2$ intensity point.

From figure 5 we can say

$$T = \frac{E_T}{E_i} \qquad (13)$$

where

E_T = the energy in the transmitted beam, and
E_i = the total energy of incident beams.

But

$$E_i = BE_R \qquad (14)$$

where

B = the beam splitter ratio, and

E_R = the energy measured by C_R.

Combining eqs (13) and (14) with eq (12) and solving for w, we get the following expression for beam radius,

$$w = a \sqrt{\frac{-2}{\ell n(1-E_T/BE_R)}} \qquad (15)$$

In the experimental setup in figure 5, E_T and E_R are measured by C_T and C_R, respectively. B is determined by E_T/E_R with the aperture wide open.

To ascertain that the beam is truly TEM_{00}, measurements of E_T and E_R are made for several different aperture sizes. If the value of w remains constant for various values of a, this confirms beam is TEM_{00}. Figure 6 shows a sample plot of beam diameter vs. aperture size at one specific point in an experimental setup.

If we wish to know the beam diameter over an extended distance along the optical axis, a series of measurements of beam diameter are made at various points over the region of interest and the results connected by some sort of smooth curve. For focused beams which converge rather rapidly (half angle > 0.01 radians) measurements should be made on both sides of the beam waist and fitted to the equation for the propagation of a TEM_{00} Gaussian beam [5]

$$w_z^2 = w_0^2 \left[1 + \left(\frac{\lambda(z-z_0)}{\pi w_0^2}\right)^2\right] \qquad (16)$$

where

w_z = the radius of the beam ($1/e^2$) at point z along the optical axis,

w_0 = the radius of the beam at the waist,

λ = the wavelength of the radiation,

z = the distance from the point of measurement to some arbitrary reference point on the optical axis (position of a beam splitter, mirror, etc.), and

z_0 = the distance from the position of the beam waist to the reference point.

Since the precise position of the beam waist is difficult to fix by visual observation, eq (16) has two unknowns, w_0 and z_0. Therefore, when fitting data from a focused beam to eq (16) by a least squares method, some of the measurements of beam diameter should be made far enough from the waist so that the curve appears linear. This permits estimation of the slope of the asymptotes, the intersection of which yields z_0. Various values of w_0 can then be tried in eq (16) and the square of the residuals from each of the least square fits plotted against w_0. The minimum of this curve yields the best estimate of w_0. For most

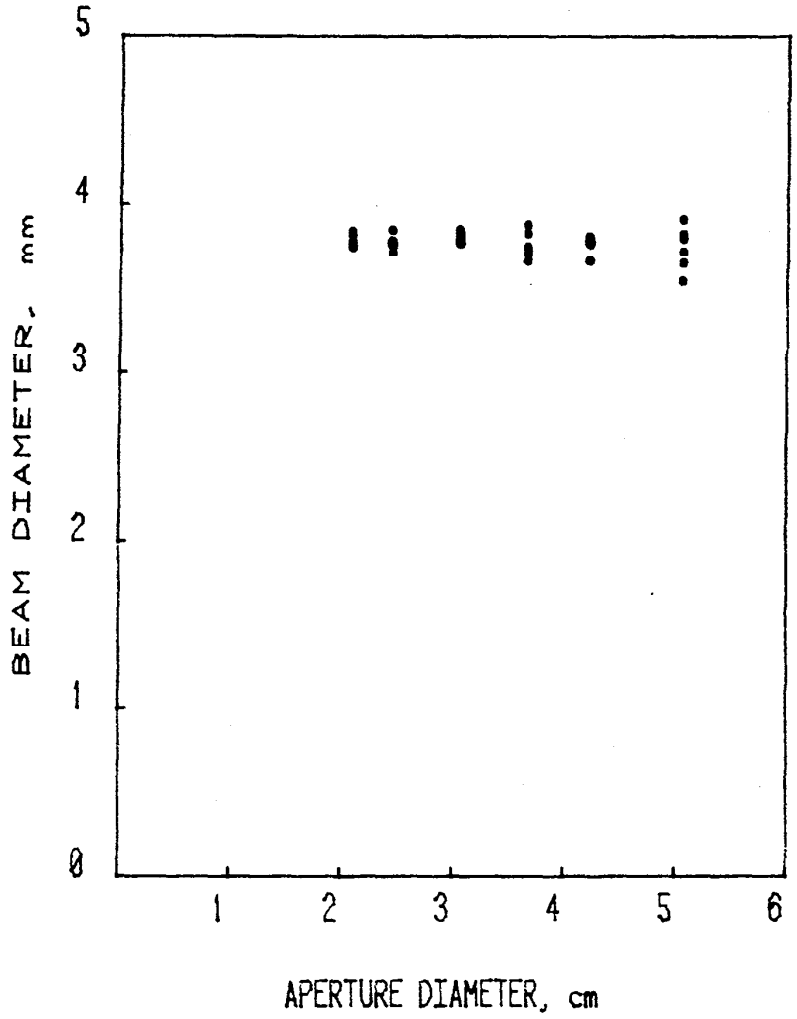

Figure 6. Plot of beam diameter vs. aperture diameter for a TEM_{00} beam.

precise results this process can be repeated for other values of z_0 close to the originally assumed value, and the w_0 and z_0 associated with the smallest value of square of the residuals used. This iterative process need only be carried on until the uncertainty in w_0 and z_0 is reduced to an acceptable value. Figure 7 is a graph showing the results of one such least squares fit.

2.5 Time Response Measurements

The time response of a detector is determined by examining its output voltage waveform. Three factors determine this function--the impulse response of the detector, the impulse response of the measuring system, and the time function of intensity of the excitation optical signal. The output waveform from the detector is a convolution of these three factors. The detector impulse response can be measured by simulating an impulse with a short optical pulse generated by some method (e.g., free induction decay [6], switching out a single pulse from a modelocked train [7]), then illuminating the detector with the impulse, and deconvolving the impulse response of the measuring system from the observed detector output.

Because the original requirement for this particular system was a verification that the detectors have a 10 ns time response, the sophisticated techniques described above were relaxed. A step function with a 10 ns risetime is degraded by a measuring system with a 1 ns risetime by only 0.5 percent assuming Gaussian transitions. Such measuring systems are readily available. Also, the need for a short impulse is obviated. A rectangular optical pulse of 10 ns duration is sufficient for the fastest excitations required and still contains enough energy to be conveniently measured. In this system such a pulse can be generated from a single longitudinal mode (SLM) TEA laser pulse with an electrooptic shutter.

Since the duration of the optical pulse is fixed, the peak power can be determined from the energy. For instance, if the rectangular pulse has a duration of 10 ns and an energy of 10 mJ, then its peak power is 100 kW. Also from the waveform data the peak voltage can be ascertained. If we divide the peak voltage by the derived peak power (100 kW in the instance above), we can arrive at a calculated responsivity. If this calculated responsivity for the short pulse is equal to that associated with longer pulses, then the time response is fast enough to cause no error; if not an error is being introduced.

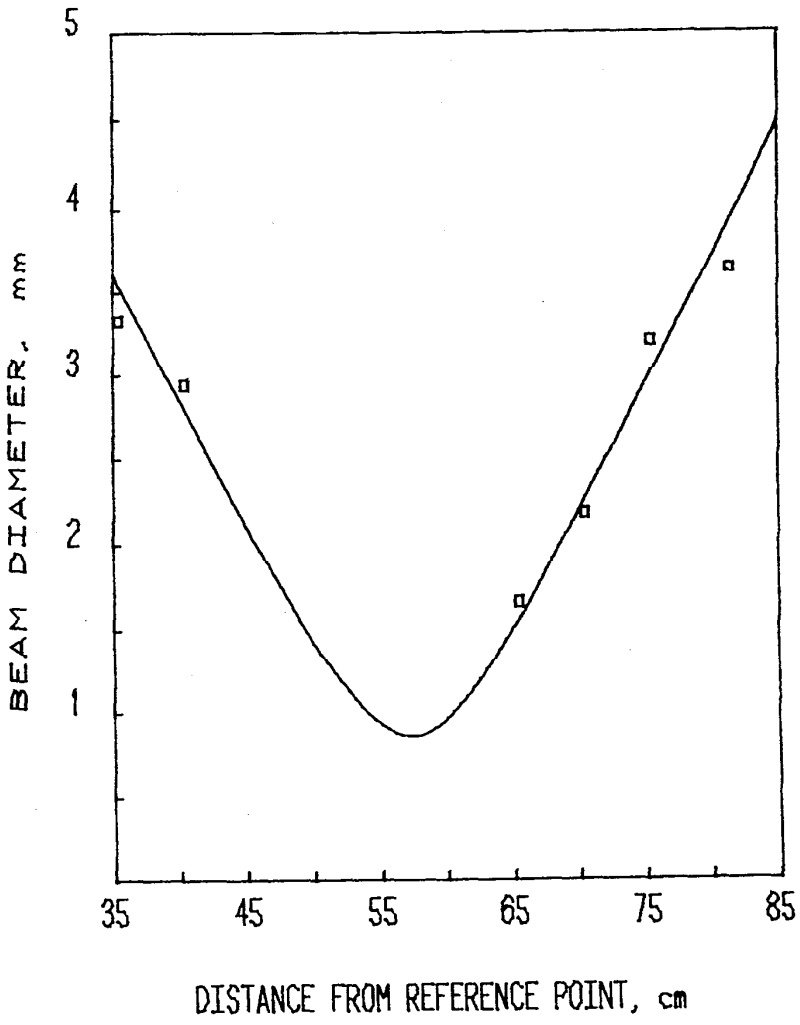

Figure 7. Plot of beam diameter as a function of distance along the optical axis.

2.6 Description of the System

There are three major parts to the system. They are:

1. the laser for generating the optical excitation pulse,
2. an arrangement of optical components for dimensioning and time-shaping the optical pulse and applying it to the detector, and
3. a computer controlled data acquisition system for running the experiment.

Figure 8 is a view of the setup of one version of the system. Often the various components are rearranged to achieve certain selected results. The three parts are described in the next three sections.

2.6.1 CO_2 TEA Laser

The laser is contained in an aluminum shielded enclosure seen in the central background of figure 8. Its power supply is located next to it. The cavity is 2.16 m long. The cell containing the gain medium is one that is commercially available. It is located within a second shield so that the emi generating components are doubly shielded. The gain medium is a mixture of 78 percent He, 12 percent CO_2 and 10 percent N_2 and is pressurized to 101 to 104 kPa (760 to 780 mm). Atmospheric pressure at Boulder is approximately 84 kPa (630 mm).

Also contained within the optical cavity is a low pressure gain cell for operating the laser at a single longitudinal mode (SLM). This cell uses the same gas mixture mentioned but at a pressure of 133 Pa (1 mm). Since this unit runs CW, a water jacket is used for cooling.

An adjustable iris is located within the cavity near the output mirror for achieving TEM_{00} operation. Output of the laser in the SLM TEM_{00} mode is approximately 200 kW and 40 mJ. With the iris wide open an SLM pulse operating with many spatial modes of nominally 1 MW and 300 mJ can be achieved.

2.6.2 Arrangement of Optical Components

The optical components are on the metal table in the foreground of figure 8. The electrooptic switch (E-O switch) is located on the mounting rail on the right side of the table and its pulse forming components are housed in the nearby screened enclosure for suppression of emi.

Figure 9 is a diagram of an alternate arrangement of optical components that was designed for adjusting the dimensional and time parameters of the optical pulse. The two objectives of this arrangement are the extraction of as little energy as possible to fire

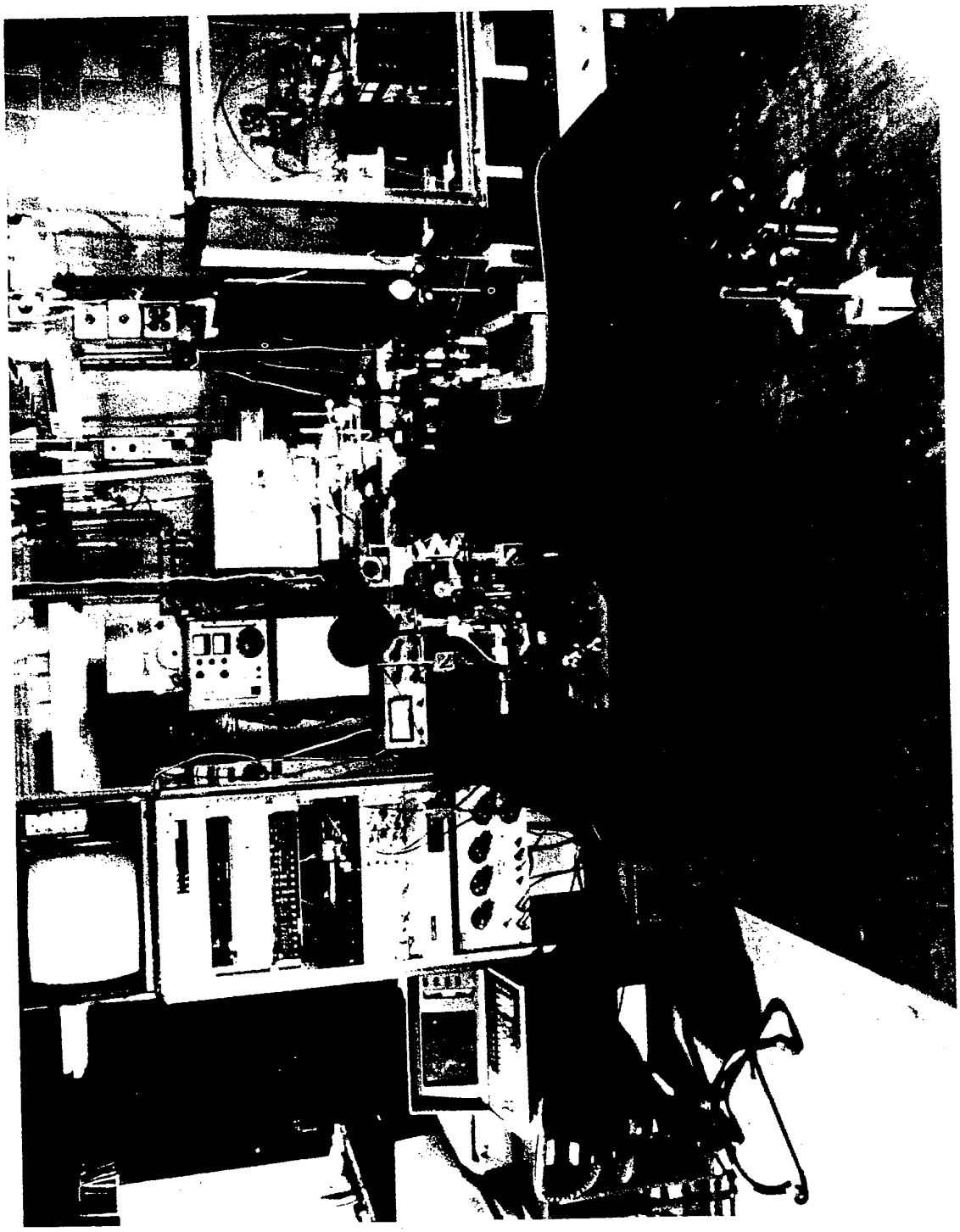

Figure 8. Pulsed CO_2 detector characterizing system.

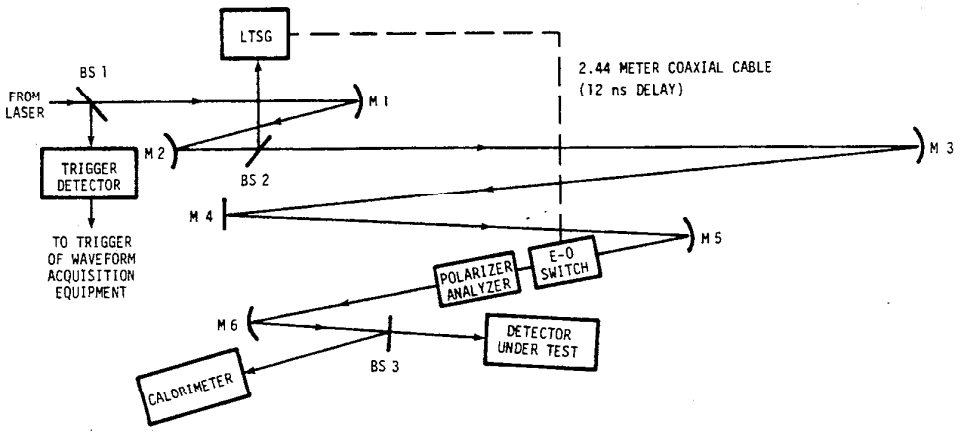

Figure 9. Arrangement of components for measuring detector characteristics.

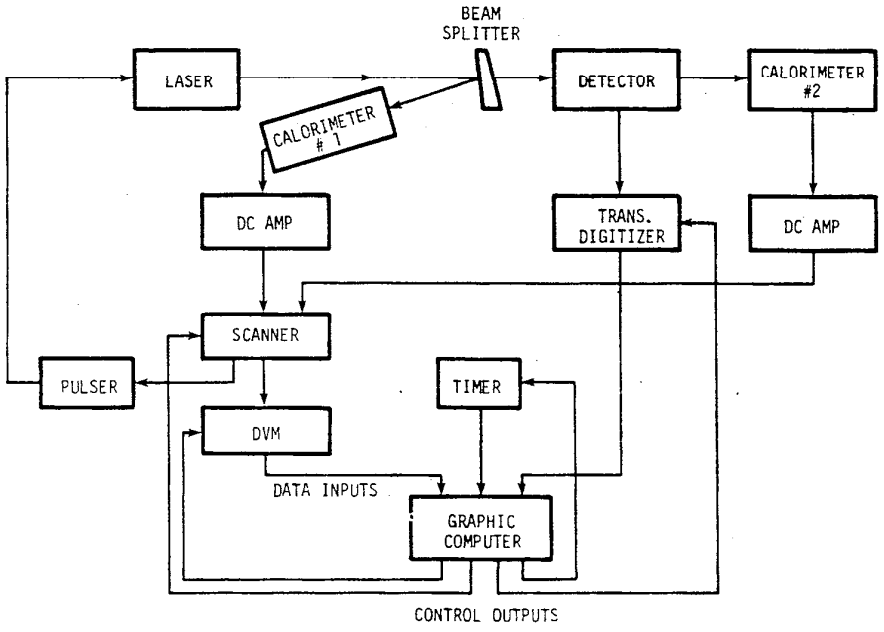

Figure 10. Block diagram of data acquisition system.

the laser triggered spark gap (LTSG), and the synchronization of the arrival times of the optical and electrical pulses at the E-O switch. The telescope formed by mirrors M1 and M2 helps achieve the first objective by reducing the laser beam diameter so that it totally fits within the entrance aperture of the LTSG. The second objective is accomplished using the optical delay line formed over the path BS2-M3-M4-M5-EO switch. This path provides the necessary 50 ns delay to allow for the LTSG to break down and for the electrical pulse to travel the coaxial line. Fine adjustment on the delay for precise synchronization is accomplished by varying the pressure on the LTSG over the range 760 to 970 kPa (110 to 140 psi) gauge pressures. M6 is used to adjust the size of the beam to fit the entrance aperture of the detector under test (DUT). Finally, the beam splitter, BS3, allows the simultaneous measurement of pulse energy and waveform. It is vital that this component be located outside the region of high irradiance of the focused beam so as to avoid damage and permit linear operation.

2.6.3 Data Acquisition System

The data acquisition system is shown to the left of the metal table in figure 8. AC power is supplied to it through an electronic regulator to reduce emi conducted over the power line as well as to enhance the precision of the measurements. Figure 10 is a block diagram of the various pieces of equipment. The arrangement shown is for feed-through detectors; for terminating detectors, calorimeter 2 and its associated amplifier can be omitted.

The graphic computer controls the experiment. It furnishes a signal through the scanner to fire the laser, and acquires and processes the data from the calorimeters and transient digitizer. Precise time intervals for making calorimeter output measurements are supplied to the computer by the timer. Final results are outputted on the screen and can be stored as hard copy or on cassette tape.

The calorimeters are a commercial, volume absorbing model with calibration factors of approximately 100 mV/J. The exact value is determined by calibrating them with the NBS K series of standards. The input aperture of these instruments is 25 mm in diameter.

The amplifiers are used to increase the output of the calorimeters for low energy signals. They are required in cases such as measuring signals in the 10 to 20 kW range or 10 ns rectangular pulses. The gain is adjustable in steps of factors of 10 over the range of 100 to 100,000. Maximum output is 10 V.

The DVM is a 6-1/2 digit instrument capable of 1 μV resolution on the most sensitive range. When controlled by the computer, readings of calorimeter output can be taken at intervals of 0.25 s, although 1 s intervals are normally sufficient.

The transient digitizer is a high-speed A to D converter with a bandwidth of 350 MHz. It is capable of resolving 1 part in 512 of full scale of the time window and the voltage range. Fastest time window is 5 ns; most sensitive voltage range is 40 mV full scale.

2.7 Measurements at High Peak Powers Above the Region of Detector Linearity

The responsivity measurement techniques in section 2.2 are limited to power levels for which the detector output voltage is a linear function of the input power. Thus, the power range is restricted to some maximum value. This maximum power value can be increased with the use of a beam splitter as shown in figure 11. The peak value in the transmitted beam is B times the peak value measured by the detector, where B is the beam splitter ratio. The only restrictions placed on this technique are that the detector continue to be operated in its linear region and that the beam splitter ratio remain unchanged at the high levels of energy.

Note that this technique delivers a calibrated beam of known peak power at a high level. This provides a vehicle for calibrating detectors in the region where their output is no longer a linear function of the input power (but is still below the damage threshold of the device). If we insert the detector in output beam as shown in figure 12 and measure the peak voltage from both detectors with two transient digitizers we can calculate the peak power on the detector experiencing the high peak power and calculate its responsivity. From figure 12 we can say

$$P_{P_b} = \frac{V_{P_a}}{R_a} \times B \qquad (17)$$

where

P_{P_b} = the peak power in W incident upon detector b,
B = the beamsplitter ratio,
V_{P_a} = the peak voltage developed by the calibrated detector a, and
R_a = the responsivity in V/W of detector a.

From this knowledge of the incident peak power on b we can say

$$R_B = \frac{V_{P_b}}{P_{P_b}} \qquad (18)$$

where

R_B = the responsivity of detector b in V/W at the high power level,
V_{P_b} = the measured peak voltage developed by detector b, and
P_{P_b} = is as in eq (17) above.

This technique determines the nonlinear effects tested for in section 2.2. It may be necessary also to perform further time response tests at high power levels.

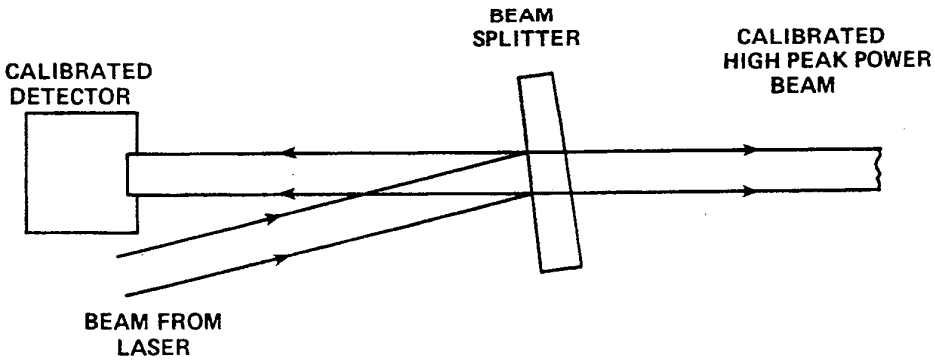

Figure 11. Arrangement of components for producing a calibrated, high peak power beam.

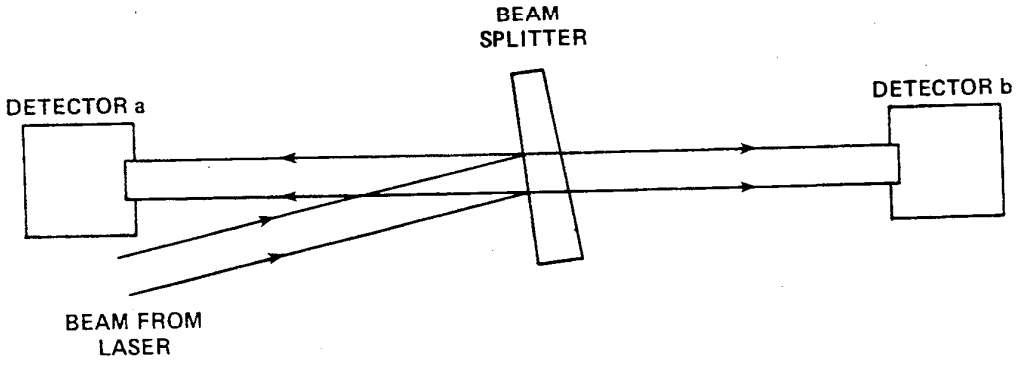

Figure 12. Arrangement of components for measuring detector responsivity in the region of nonlinear operation.

3. Tests on Selected Detectors

3.1 General Remarks Concerning Detector Tests

The tests described in the following sections of this chapter were performed as part of a program to identify a room temperature operating device that was a promising candidate for a transfer standard for CO_2 TEA laser peak power. Not all the previously mentioned tests were performed on each of the units as some were eliminated early because of various drawbacks for this specific application. However, the following sections do give specific examples of the measurements discussed in chapter 2.

3.2 Pyroelectric Detectors

Pyroelectric detectors listed as stock items from two manufacturers plus one laboratory model were studied. The dimensions of these detectors were of the order of 1 mm square. All units were capable of resolving modelocking spikes but the commercial models exhibited a mechanical ringing resulting from piezoelectric effects. This undesirable ringing, readily apparent in figure 13, persisted for several microseconds beyond the cessation of the optical pulse and caused large distortions in the output waveform. The laboratory model appears to be adequately damped as there is no ringing visible in its output which is shown in figure 14.

Pyroelectric detectors of the above size are restricted to only moderate pulse energies, their upper limit being approximately 10 mJ. Thus, for pulses with an equivalent duration[2] of 200 ns, the maximum peak power is 50 kW. To measure higher powers some form of a calibrated attenuator must be employed ahead of the device.

The small aperture size, typically 1 mm square, also accentuates the problems associated with total beam capture discussed in section 2.2. Because of these shortcomings extensive measurements on this type of detector were not performed.

---

[2]Equivalent duration is defined as duration of a rectangular pulse having the same peak power and energy as the pulse in question.

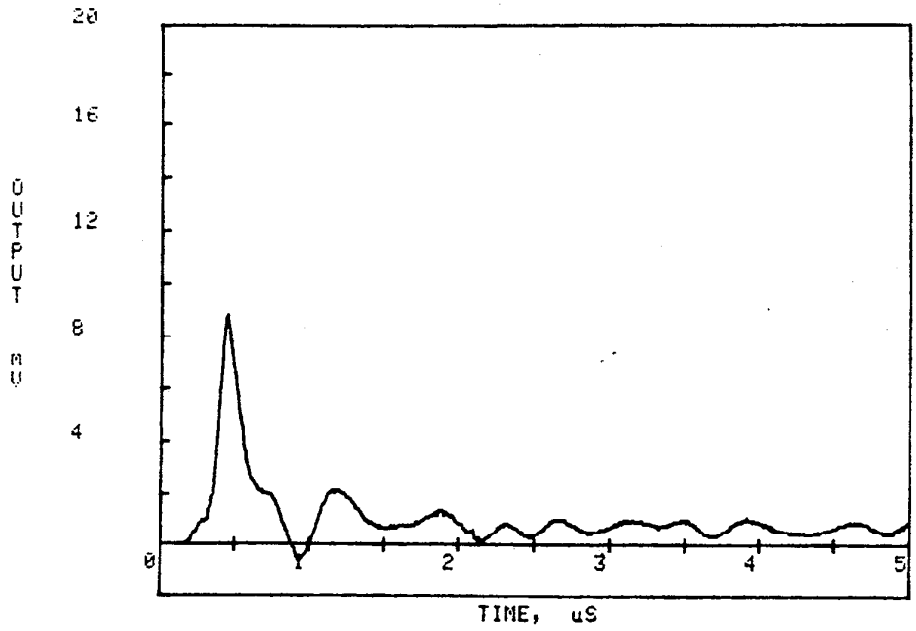

Figure 13. Output response of a commercially available pyroelectric detector.

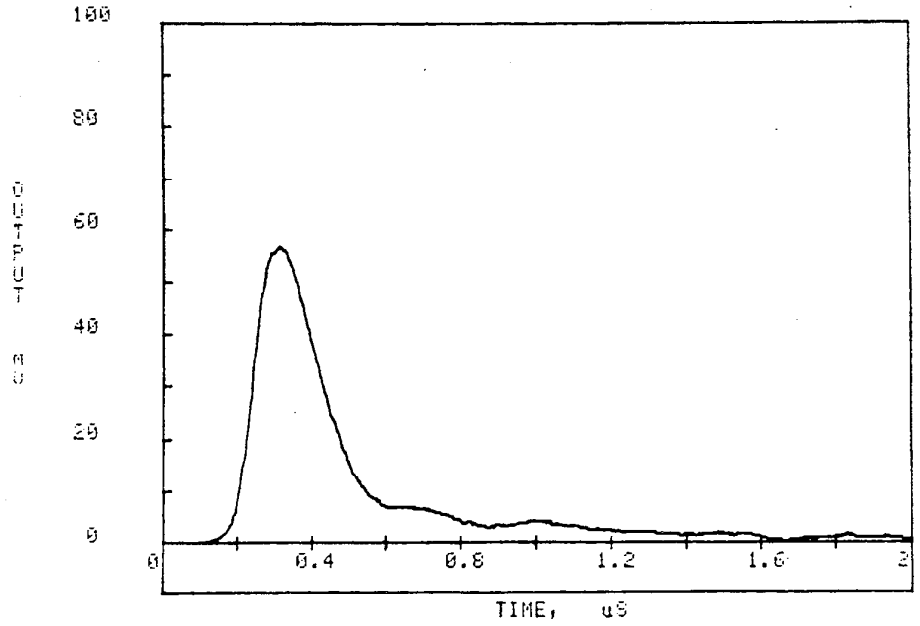

Figure 14. Output response of a laboratory model pyroelectric detector.

3.3 Photon Drag Detectors

The photon drag detectors discussed in this section are terminating (beam absorbing) type units as opposed to the feed-through units discussed in the next section. All had apertures of 20 mm^2, two being circular with a 5 mm diameter and one square, 4.5 mm on a side.

The theoretical time response of this type of detector is extremely fast, being less than 1 ns and approximately equal to the time of flight of photons through the material [8]. However, less than ideal mounting configurations and poor impedance matching to external circuitry can degrade these fast transition times.

All the detectors resolved modelocking spikes and exhibited good waveform reproduction. Figure 15 shows the response of one of the detectors to an SLM pulse. The time response of this detector was measured by the method discussed in sections 2.5 and 2.6.2. Figure 16 shows the detector response to a 10 ns "rectangular" pulse. The noise along the baseline results from electrical reflections caused by impedance discontinuities in the coaxial transmission line from the LTSG and in the E-O switch head. These electrical reflections prevent the E-O switch from turning off in a clean manner. (Subsequent improvements have significantly reduced these perturbations.) The responsivity derived from the 10 ns pulses was

$$7.72 \times 10^{-4} \text{ V/kW} \pm 6.1\%.$$

This value compares quite favorably with a responsivity of

$$7.61 \times 10^{-4} \text{V/kW} \pm 2.1\%,$$

which was measured for pulses similar in shape to that in figure 15. The ± values quoted in this section and also 3.4 are estimates of imprecision based on the standard deviation of the mean [9]. They have had Student's t distribution applied and are the 95% confidence values.

The greater imprecision associated with the 10 ns pulses resulted from two sources: misalignment of the detector and decrease in signal to noise in the energy measurement. The beam misalignment resulted from a slight deviation in the beam position when the polarizer-analyzer was rotated to the extinction position. The small energy in the 10 ns pulse was insufficient to give a visible indication of beam location, so the detector was repositioned to obtain maximum output as a means of correcting the alignment. By far the greatest imprecision was caused by the 20-fold reduction in energy. For the total pulse the energy was typically 10 mJ, while the 10 ns pulse contained 0.5 mJ. The actual measured values of these energies are one-fourth the above values since they are attenuated by the beam

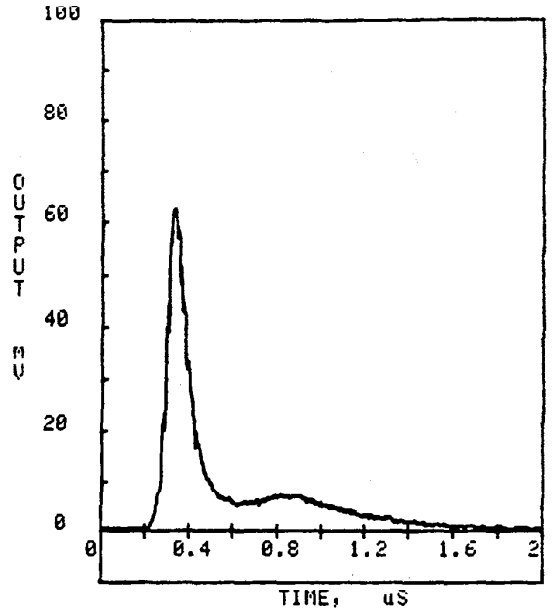

Figure 15. Output response of a photon drag detector to an SLM TEA laser pulse.

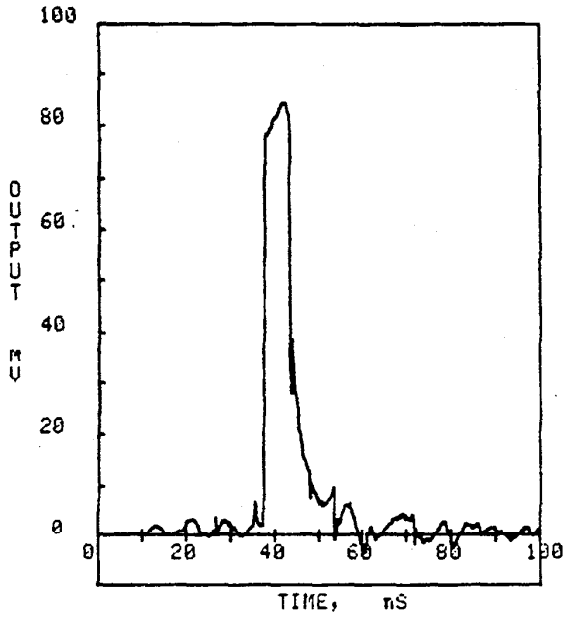

Figure 16. Photon drag detector response to a 10 ns sample extracted from an SLM TEA laser pulse.

splitter ratio. The measurement of this low energy by the calorimeter was somewhat sensitive to random changes in ambient conditions occurring during the measurement period.

3.4 Photon Drag Monitors

These units are similar to the photon drag detectors in section 3.3 but have the added property of being feed-through devices. They also have larger apertures than the detectors in 3.3. Three monitors were studied in this section, one having input and output apertures 12.7 mm in diameter and the other two detectors 25.4 mm in diameter. These large apertures greatly simplify the beam capture problems described earlier but do introduce a new complication, namely a spatial dependence of responsivity.

This variation of responsivity over various portions of the detector surface is readily apparent to the observer. As he moves the laser beam from the center towards the edge of the monitor the voltage output increases an appreciable amount. This phenomenon can produce confusing results if pulsed beams of equal peak power impinge on different areas of the detector, or are coaxial but of differing diameters, or are coaxial and of the same diameter but possess different spatial mode structure. This effect can be minimized by limiting the beam to a region near the center of the detector where spatial variations are small.

The output responsivity of the two 25.4 mm monitors at several positions was measured. A collimated TEM_{00} SLM beam, 4.8 mm in diameter, served as a probe. A calorimeter placed close to the output aperture measured the output energy for the responsivity determination. No beam splitter was required.

Figure 17 shows the results of measurements on one detector. The other detector possessed similar characteristics. The circles represent areas containing 99% of the power in the beam; the numbers are the measured values of output responsivity in V/MW. The peak power in the exit beam was in the range 150 kW to 220 kW for this series of measurements. The imprecision of the measurements at the center is ± 5% while at the edges it increases to a maximum of ± 11%. Systematic error in both cases is 4.5%. (See chapter 4, Error Analysis, for a discussion of systematic errors.)

The insertion loss of the two monitors was measured using the tandem method described in section 2.3 and depicted in figure 4. As previously mentioned the polarity of the output of photon drag detectors is dependent on the direction of photon flow through the device so a check was made to verify that any reflected light from the "b" device in figure 4 did not reduce the voltage output of "a". A sheet of teflon, which is a good volume absorber for 10.6 μm radiation [10], was inserted between the two monitors. No change in output waveform from monitor "a" could be detected, which is consistent with the fact that the devices are AR coated.

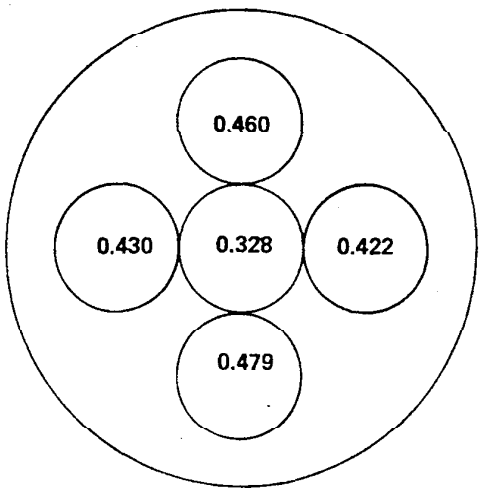

Figure 17. Output responsivity of a feed-through photon drag detector at various locations on the surface.

The insertion loss as determined from eq (11) was 1.26, which from eq (5) gives an input responsivity, S_i, of 0.289 V/MW. The imprecision for these measurements is 10%.

A power linearity check was made on the monitor with the 12.7 mm apertures. The output responsivity was measured at various output power levels over the range 37 kW to 185 kW. The lower levels were generated by attenuating the beam by using the front surface reflection off a wedged zinc selenide beamsplitter. Over this range the output responsivity was 0.208 V/MW with an imprecision of 3.9%.

4. Error Analysis

4.1 General Discussion of Errors

The sources of error can be determined by considering the basic principle of the system as discussed in chapter 2. We need to determine the errors associated with measurement of the optical energy and those associated with waveform voltages. The error contributed by each measuring device will be considered separately and then the reader can derive the total error for a particular measurement configuration by considering the effect of just those components used. The uncertainties quoted in this section are based on calibrations made with random errors estimated at the 95% confidence level.

4.2 Energy Measurement Errors

The energy is measured with commercially available, volume absorbing calorimeters. These units were calibrated against the NBS K series calorimetric standard [11]. The uncertainty associated with the calibrations is ± 3%.

The calorimeters were subjected to fluences of approximately 5 J/cm^2 and no departure from linear operation could be detected. Since the units are usually placed where the beam diameter is 5 mm or greater and since the incident energy very seldom exceeds 180 mJ for a TEM_{00} beam, calorimeter linearity is not a problem.

The energy measurement is also dependent upon the gain accuracy of the dc amplifier (when it is in the system) and the DVM. Calibrations of these two instruments show they are well within their manufacturer's quoted specifications of 0.01% and 0.002%, respectively, and therefore have a negligible effect on the uncertainty.

In summary, the error in the energy measurement is ± 3%.

4.3 Beam Splitter Ratio Errors

A beam splitter is required in this system when measuring energy incident upon a detector (except in the tandem monitor configuration of section 3.4). The units used in this system are made of zinc selenide. They have uncoated surfaces which form a wedge having an apex angle of 1°. Danielson and Beers [12] have shown that this type of device serves as an accurate, calculable energy or power sampling device, the exact ratio of the sample energy to that in the main beam being dependent upon the index of refraction of the material, the wedge angle, the order of the reflection, and the angle of incidence of the laser beam. The ratio of transmitted energy to that from the front surface reflection was measured by a method outlined in [13] to confirm that no serious defects were present in the units to cause departures from the theoretical ratios. The uncertainty associated with the beamsplitter ratio is ± 0.5%.

The beam splitters were checked for linear operation by observing the ratio while subjecting them to various values of fluence. At fluences up to approximately 5 J/cm^2 (25 MW/cm^2) no departures from linear operation could be detected. Above that value erratic operation was noted and at times a faint flashing on the surface noted. At 20 J/cm^2 (100 MW/cm^2) surface damage was produced. As a result the maximum fluence to which they are subjected is kept below the 5 J/cm^2 value.

4.4 Waveform Measurement Errors

The time function of output voltage from the detector is measured by the transient digitizer. This instrument is capable of resolving each time and voltage range with a precision of 1 part in 512. The bandwidth of the instrument is 350 MHz. This instrument was calibrated by Young and Lawton [14] with an uncertainty of ± 1.5%.

4.5 Beam Diameter Measurement Errors

Beam diameter measurements are made with an adjustable iris as discussed in section 2.4. Errors in this measurement can arise from various sources. When determining the diameter at one location along the optical axis these sources can include such factors as misalignment of the beam through the center of the aperture, inaccuracy in setting the aperture diameter, nonrepeatability of laser beam characteristics and noise in the measurement system. If the aperture size and position are reset prior to each measurement, the errors will tend to be randomized and the standard deviation will give an idea of the uncertainty of the measurement. For measurements of beam diameter along an extended distance of the optical axis, the closeness of fit of the individual points to the theoretically predicted equation gives an idea of the uncertainties involved.

The contribution to the total uncertainty of the measurement of detector responsivity by errors in the beam diameter measurement will vary depending on the ratio of the aperture size to beam diameter. Obviously, if the detector aperture diameter is much greater than the beam diameter larger errors can be tolerated. Figure 18 shows the uncertainty introduced into the transmittance of a circular aperture as a function of the relative sizes of the aperture and the TEM_{00} beam. Curves are shown for three values of uncertainty in the beam diameter measurement. Figure 19 shows the same information for square apertures. A derivation of an expression for the transmittance of a square aperture for a TEM_{00} Gaussian beam is given in the Appendix. From the curves presented one can see that errors in beam diameter measurements can result in uncertainties ranging from negligible for apertures twice as big as the beam diameter to nearly 10% when the aperture and beam diameter are equal.

4.6 Time Response Measurement Errors

In this section we shall present data to give the reader some feel for the risetimes that can be measured using a 10 ns rectangular optical pulse to excite the detector as described in section 2.5. From this it will be seen that the waveform shown in figure 16 results from a detector with a very fast time response--much faster than 10 ns.

Figure 20 through 25 are computer generated plots showing the convolution of a 1 V, 10 ns rectangular pulse with various duration Gaussian impulse responses. This type of impulse response was chosen as an example because many mechanisms in nature exhibit, to a first approximation, a Gaussian response. From the curves we can see that detectors having a Gaussian impulse response with duration greater than 3 ns will exhibit a lowering of the output when excited with a 10 ns rectangular pulse. When the impulse response duration is 7 ns, the loss in output is nearly 10%. Also, the nearly straight and parallel sides in figure 20 are quite similar to those in figure 16, indicating a detector time response of the order of magnitude of 1 ns.

4.7 Summary of Error Analysis

The errors associated with the various sources of systematic error are as follows:

Energy Measurement	3.0%
Beamsplitter Ratio	0.5%
Waveform Measurement	1.5%

For each experiment, the error in the measurement of beam diameter must be determined from figure 18 or 19. It will generally lie in the range 0.0 to ± 10% depending on the precision of the measurements and the size of the detector aperture compared to the beam diameter.

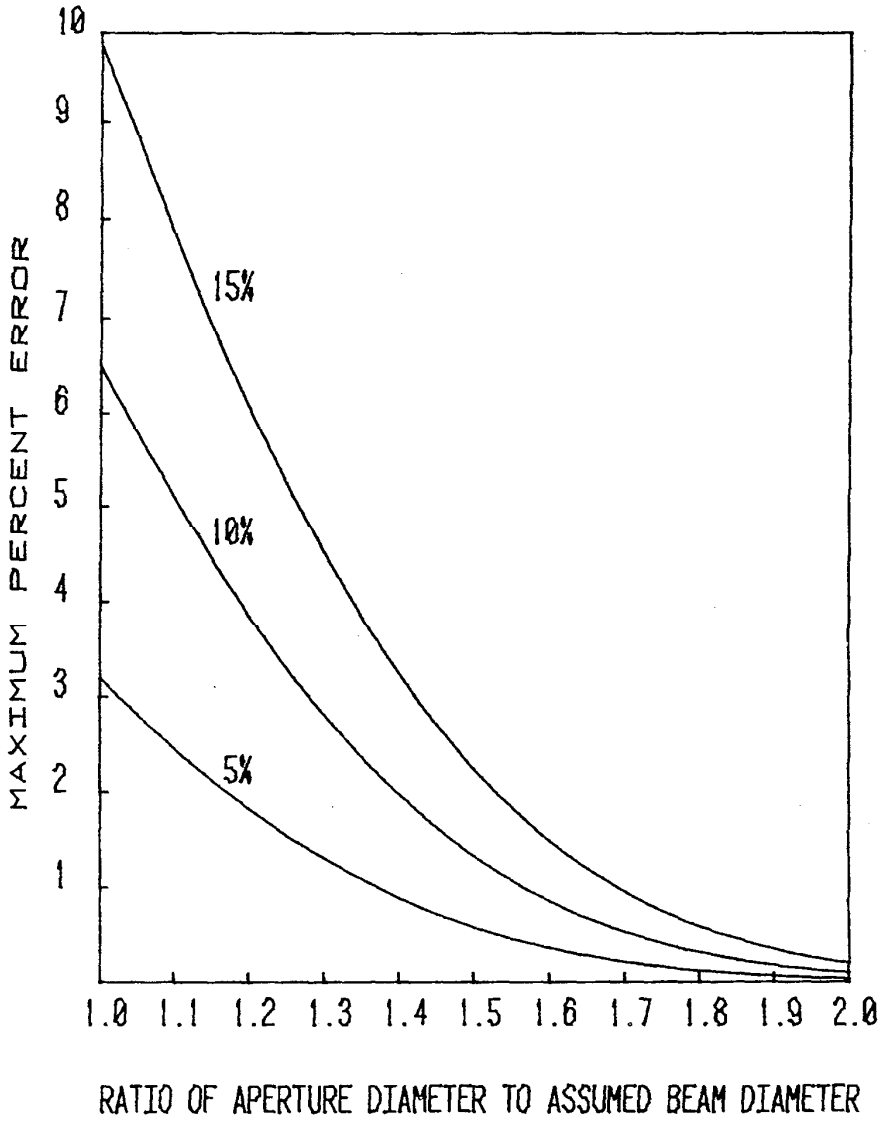

Figure 18. Maximum possible error in the transmittance of a circular aperture contributed by the uncertainty of the beam diameter measurement. The percent value shown by each curve identifies the uncertainty in the beam diameter measurement. The ordinate is the maximum percent error in the transmittance.

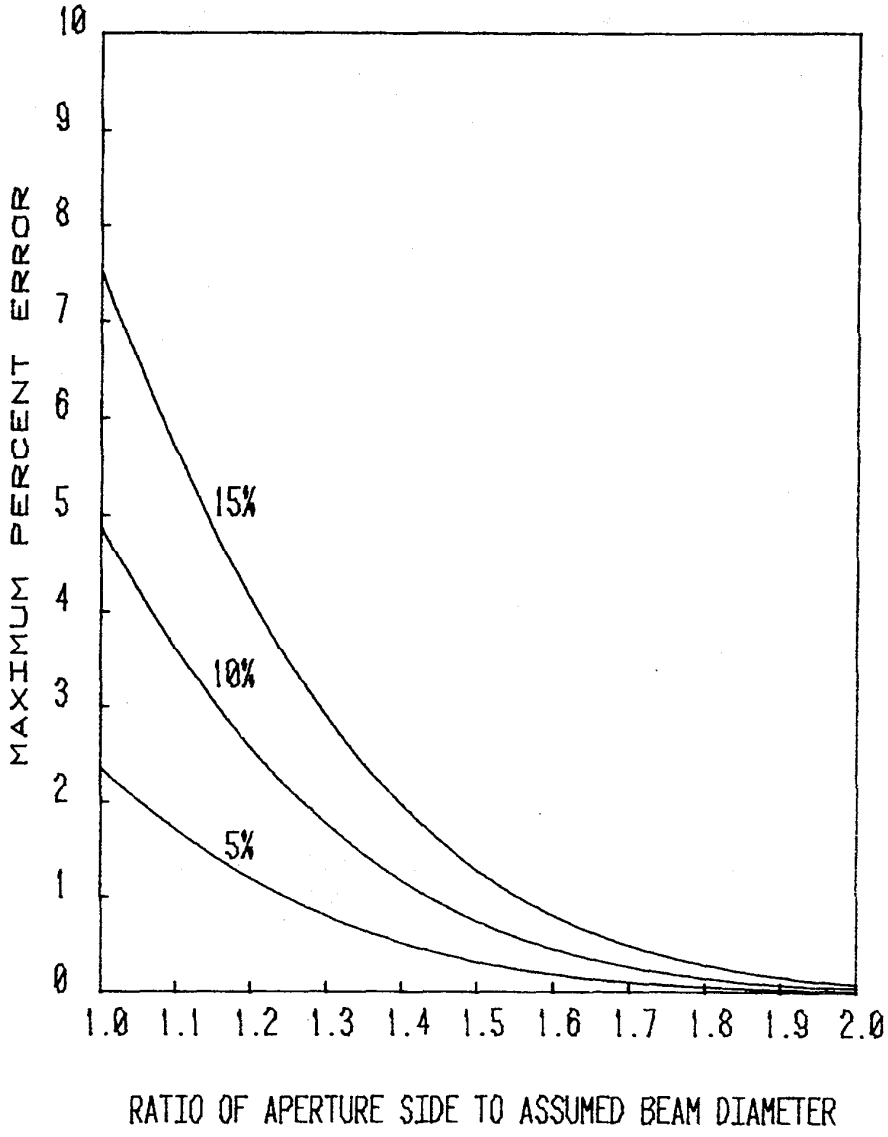

Figure 19. Maximum possible error in the transmittance of a square aperture contributed by the uncertainties of the beam diameter measurement. The percent value shown by each curve identifies the uncertainty in the beam diameter measurement. The ordinate is the maximum percent error in the transmittance.

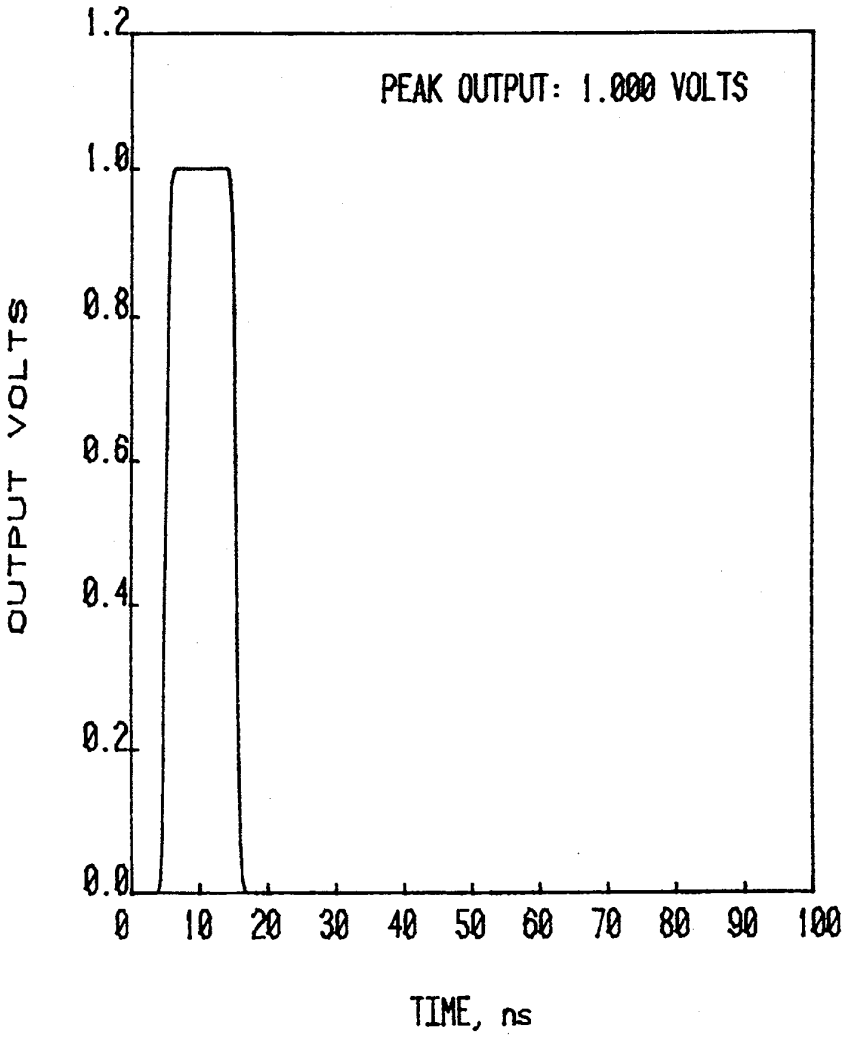

Figure 20. Convolution of a 1 volt 10 ns rectangular pulse with a unit area Gaussian pulse of 1 ns duration (FDHM). The peak value of the resultant waveform is 1.000 V.

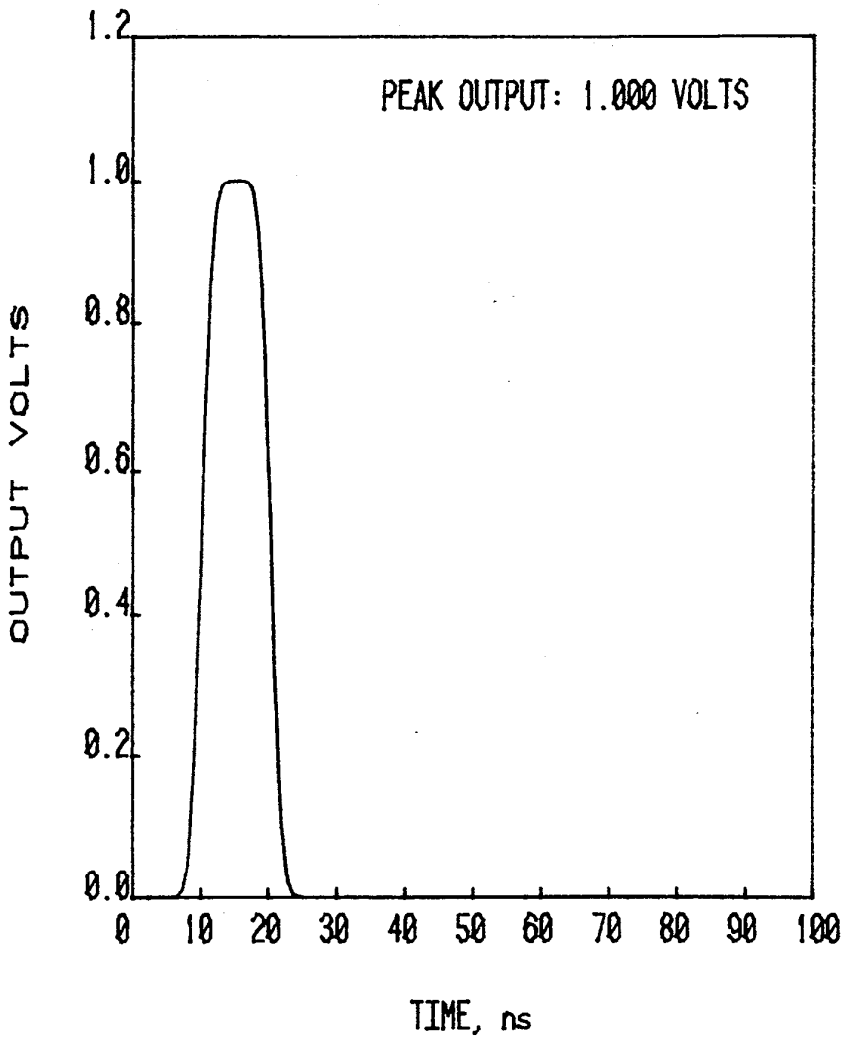

Figure 21. Convolution of a 1 volt 10 ns rectangular pulse with a unit area Gaussian pulse of 3 ns duration (FDHM). The peak value of the resultant waveform is 1.000 V.

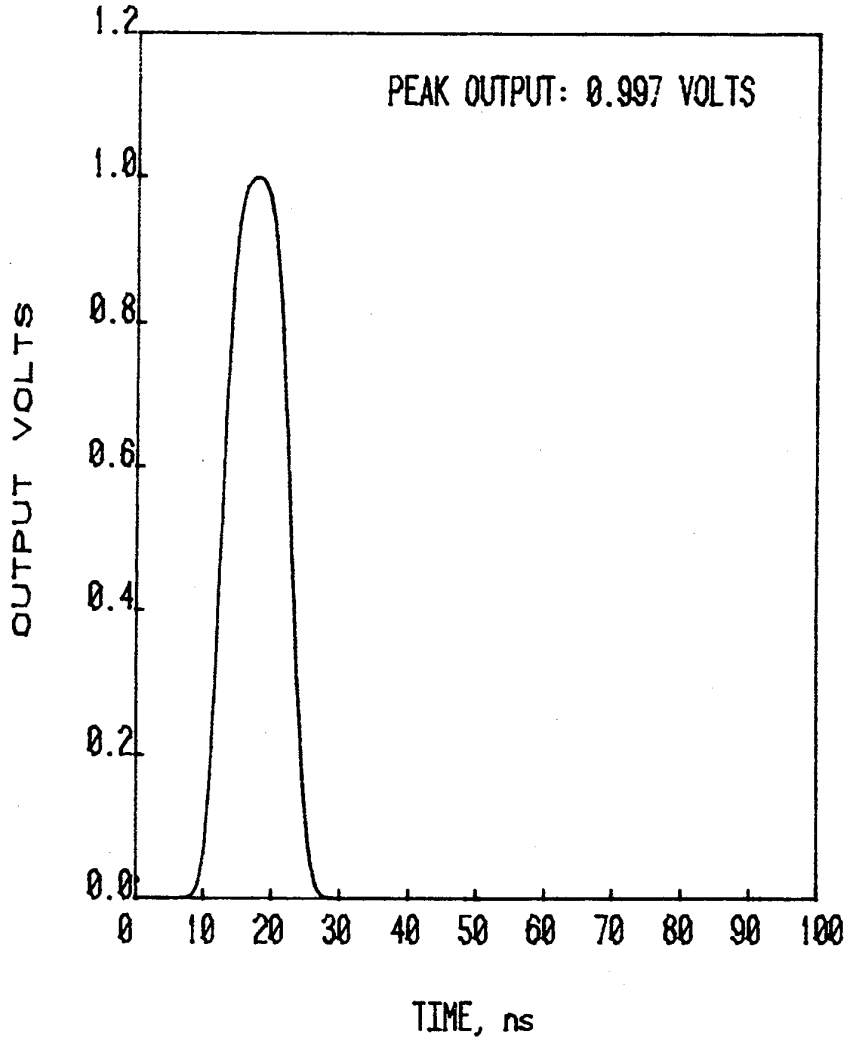

Figure 22. Convolution of a 1 volt 10 ns rectangular pulse with a unit area Gaussian pulse of 4 ns duration (FDHM). The peak value of the resultant waveform is 0.997 V.

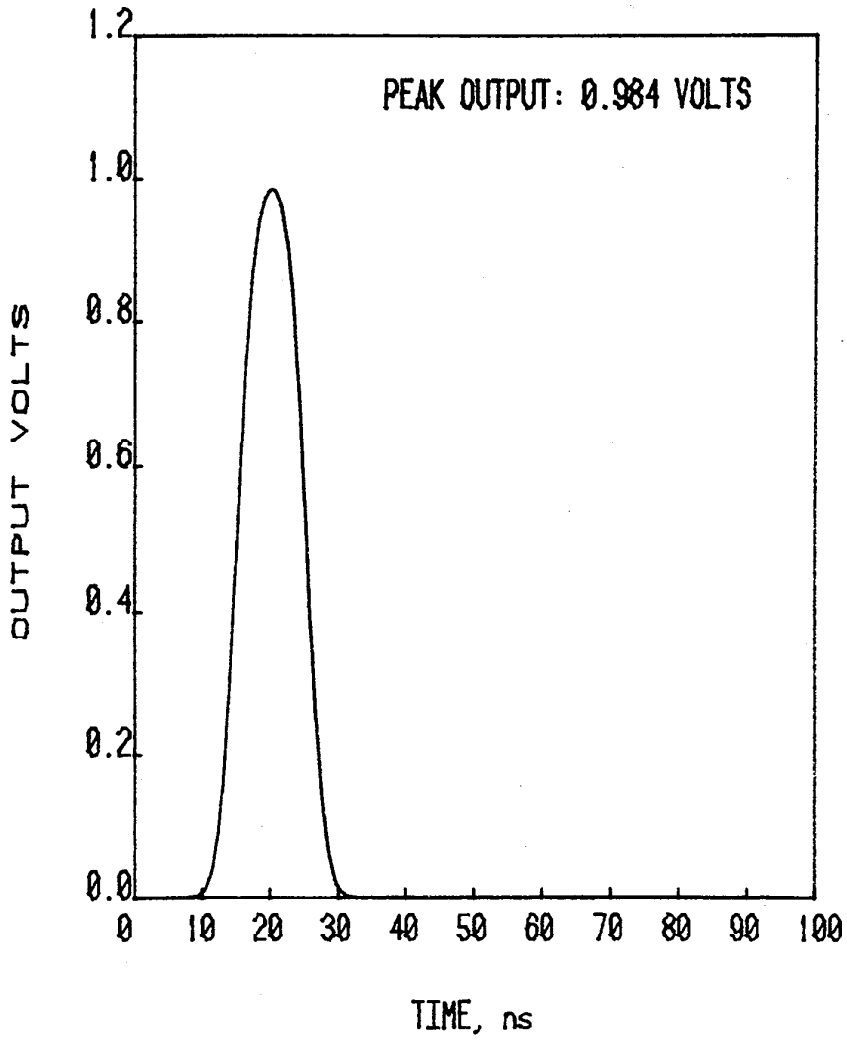

Figure 23. Convolution of a 1 volt 10 ns rectangular pulse with a unit area Gaussian pulse of 5 ns duration (FDHM). The peak value of the resultant waveform is 0.984 V.

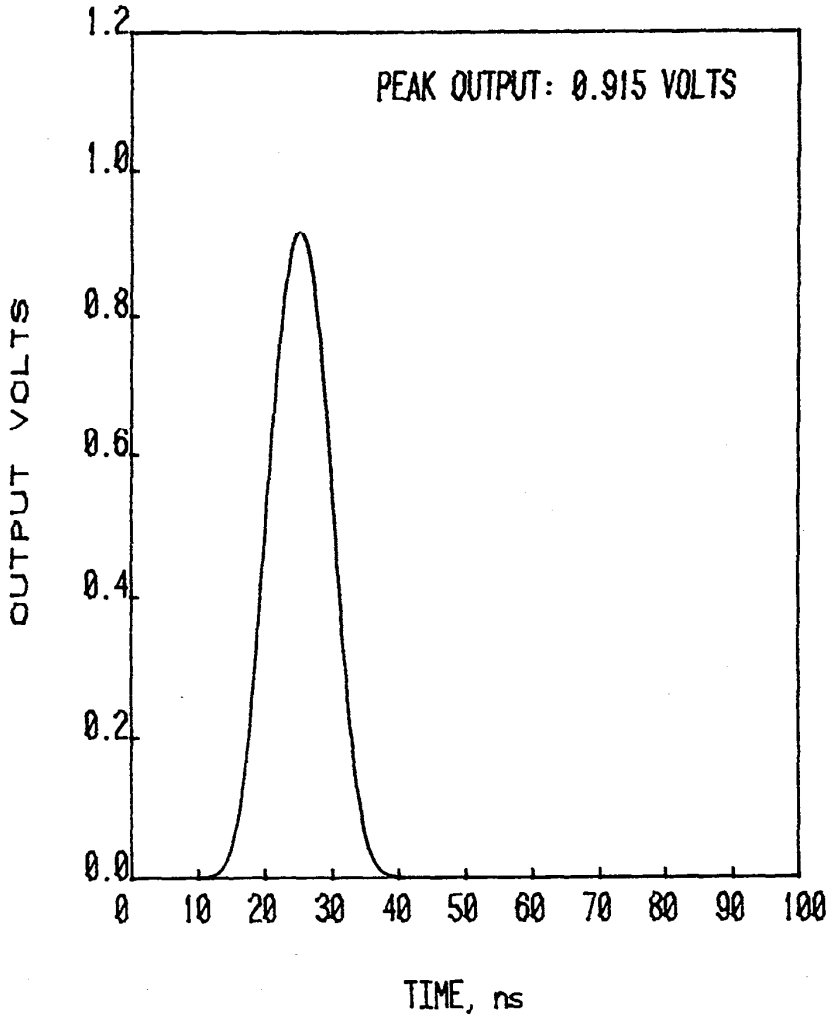

Figure 24. Convolution of a 1 volt 10 ns rectangular pulse with a unit area Gaussian pulse of 7 ns duration (FDHM). The peak value of the resultant waveform is 0.915 V.

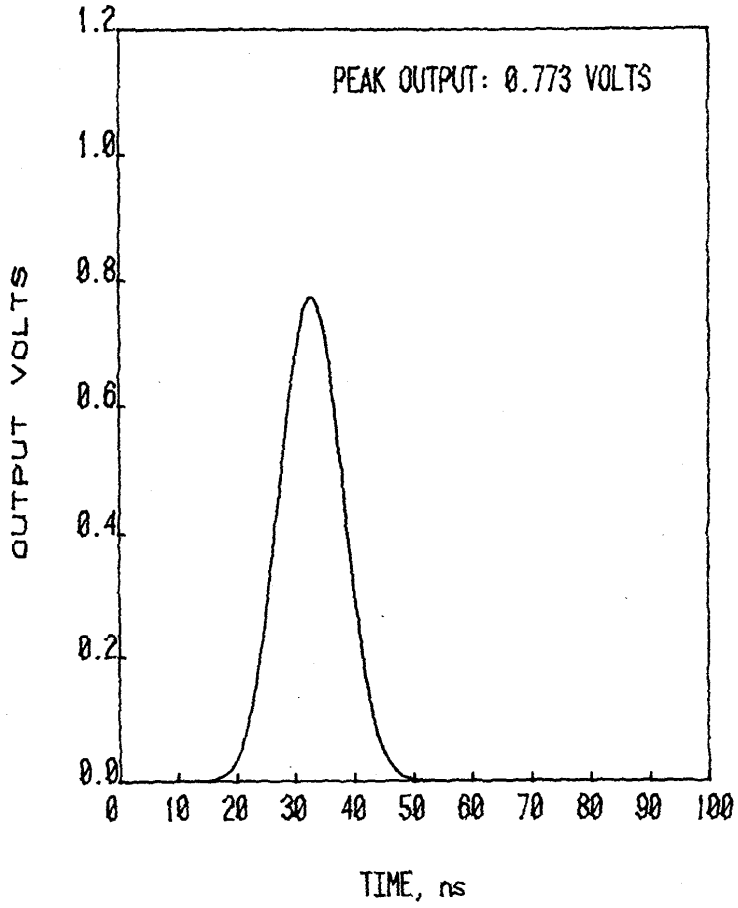

Figure 25. Convolution of a 1 volt 10 ns rectangular pulse with a unit area Gaussian pulse of 10 ns duration (FDHM). The peak value of the resultant waveform is 0.773 V.

To these systematic errors summarized in this section must be added the random errors associated with the individual determinations of energy to arrive at the total uncertainty.

5. Conclusions

A system for measuring the responsivity of detectors of high peak power pulsed 10.6 μm radiation has been developed. By using calibrated beam splitters the methods used are extendable into power ranges where the detectors no longer respond to power in a linear manner. The insertion loss of feed-through detectors can also be measured. A method has also been developed to test detectors for response times faster than 10 ns. A technique is also explained for measuring the diameter of TEM_{00} Gaussian laser beams.

6. Appendix: Transmittance of a Gaussian Beam Through a Square Aperture

We assume the irradiance in the beam is given by

$$I = I_0 \, e^{-\frac{2}{\sigma^2}\left[(x-x_0)^2 + (y-y_0)^2\right]} \tag{A-1}$$

where

I = the irradiance at point x,y,
I_0 = the maximum irradiance,
σ = the "beam size" parameter,
x,y = the coordinates of the point in question,
x_0,y_0 = the center coordinates of the aperture relative to the center of the laser beam.

We also postulate the aperture is square with dimensions a x a. The power, P, accepted by the aperture is given as

$$P = I \int_{x_0-\frac{a}{2}}^{x_0+\frac{a}{2}} dx \int_{y_0-\frac{a}{2}}^{y_0+\frac{a}{2}} dy \; e^{-\frac{2}{\sigma^2}(x^2+y^2)} \tag{A-2}$$

We have the following integral in "x" plus a like one in "y".

$$J(\sigma,x_0,a) = \int_{x_0-\frac{a}{2}}^{x_0+\frac{a}{2}} e^{-\frac{2}{\sigma^2}x} \, dx \tag{A-3}$$

If we let $t = x\sqrt{2}/\sigma$, then

$$J(\sigma,x_0,a) = \frac{\sigma}{\sqrt{2}} \int_{\frac{\sqrt{2}}{\sigma}(x_0-\frac{a}{2})}^{\frac{\sqrt{2}}{\sigma}(x_0+a)} e^{-t^2}\, dt \,, \qquad \text{(A-4)}$$

$$= \frac{\sigma}{\sqrt{2}} \int_0^{\frac{\sqrt{2}}{\sigma}(x_0+\frac{a}{2})} e^{-t^2}\, dt + \int_0^{\frac{\sqrt{2}}{\sigma}(-x_0+\frac{a}{2})} e^{-t^2}\, dt \,, \qquad \text{(A-5)}$$

$$= \frac{\sigma}{\sqrt{2}} \frac{\sqrt{\pi}}{2} \left[\operatorname{erf} \frac{\sqrt{2}}{\sigma}(x_0+\frac{a}{2}) + \operatorname{erf} \frac{\sqrt{2}}{\sigma}(-x_0+\frac{a}{2}) \right] \qquad \text{(A-6)}$$

where erf denotes the error function.

A similar expression can be derived in terms of y and the final expression for the power transmitted is the product of eq (A-6) and its y counterpart. Thus, power transmitted through the aperture is

$$P = I_0 \frac{\pi\sigma^2}{8} \left[\operatorname{erf} \frac{\sqrt{2}}{\sigma}(x_0+\frac{a}{2}) + \operatorname{erf} \frac{\sqrt{2}}{\sigma}(-x_0+\frac{a}{2}) \right]$$

$$\times \left[\operatorname{erf} \frac{\sqrt{2}}{\sigma}(y_0+\frac{a}{2}) + \operatorname{erf} \frac{\sqrt{2}}{\sigma}(-y_0+\frac{a}{2}) \right] \qquad \text{(A-7)}$$

Eq (A-7) gives the power transmitted if the peak irradiance is known. The transmittance of the aperture can be derived by recalling the total power in the beam is

$$P_t = I_0 \frac{\pi\sigma^2}{2} \,, \qquad \text{(A-8)}$$

and dividing eq (A-7) by eq (A-8) yields

$$T_c = \frac{1}{4} \left[\operatorname{erf} \frac{\sqrt{2}}{\sigma}(x_0+\frac{a}{2}) + \operatorname{erf} \frac{\sqrt{2}}{\sigma}(-x_0+\frac{a}{2}) \right] \times$$

$$\left[\operatorname{erf} \frac{\sqrt{2}}{\sigma}(y_0+\frac{a}{2}) + \operatorname{erf} \frac{\sqrt{2}}{\sigma}(-y_0+\frac{a}{2}) \right] \qquad \text{(A-9)}$$

where T_0 = the transmittance.

A computer program can be developed for a solution to eqs (A-7) and (A-9) by recalling that erf(z) = -erf(-z) and employing the following approximation from reference 15.

$$\mathrm{erf}(z) = 1 - \frac{1}{(1+a_1z+a_2z^2+a_3z^3+a_4z^4+a_5z^5+a_6z^6)^{16}} \qquad \text{(A-10)}$$

where

a_1 = .07052 30784
a_2 = .04228 20123
a_3 = .00927 05272
a_4 = .00015 20143
a_5 = .00027 65672
a_6 = .00004 30638

This approximation has an error no greater than 3×10^{-7}.

7. Acknowledgments

The author wishes to thank Eric Johnson for invaluable help in deriving many of the mathematical solutions that form the basis for this work. Also special thanks to Doug Franzen for his helpful suggestions while the laser was being built. Finally, thanks to Aaron Sanders, Bruce Danielson, Bill Case, Leonard Schmidt, and Joe Skudler for their assistance at various times during this endeavor.

8. References

1. Jacobs, S. F., et al., Laser induced fusion and x-ray laser studies, Addison Wesley Publishing Co., Inc., Reading, MA (1976).
2. Glass, Alexander J., and Guenther, Arthur H., Laser induced damage in optical materials: 1978, NBS Special Publication 541 (Dec. 1978).
3. Danishevskii, A. M., et al., Dragging of free carriers in direct interband transitions in semiconductors, Soviet Physics JETP, 31, No. 2, pp. 292-295 (Aug. 1970).
4. Kogelnik, H., and Li, T., Laser beams and resonators, Proc. IEEE, 54, No. 10, p. 1317 (Oct. 1966).
5. Kogelnik, H., and Li, T., Laser beams and resonators, Proc. IEEE, 54, No. 10, p. 1315 (Oct. 1966).
6. Yablonovitch, Eli, Short CO_2 laser pulse generation by optical free induction decay, Applied Physics Lett., 25, No. 10, p. 580 (15 November 1974).
7. Champagne, L. F., et al., A large aperture CdTe Pockels cell for CO_2 lasers, Optics Communications, 13, No. 3, pp. 282-285 (Mar. 1975).
8. Kimmitt, M. F., et al., Photon drag radiation monitors for use with pulsed CO_2 lasers, J. Phys. E.: Scientific Instruments, 5, p. 239 (1972).
9. Brownlee, K. A., Statistical theory and methodology in science and engineering, John Wiley & Sons, p. 80 (1965).
10. Gunn, Stuart R., Studies of calorimeter absorbers for CW and pulsed CO_2 lasers, Lawrence Livermore Lab., Rept. UCRL 51854 (1975).
11. West, E. D., and Schmidt, L. B., A system for calibrating laser power meters for the range 5-1000 W, NBS Technical Note 685 (May 1977).
12. Danielson, B. L., and Beers, Y., Laser attenuator for the production of low power beams in the visible and 1.06 μm regions, NBS Technical Note 677 (Jan. 1976).
13. Case, W. E., Quality assurance for the NBS C, K, and Q laser systems, NBSIR-1619 (Aug. 1979).
14. Young, M., and Lawton, R. A., Measurement of pulsed laser power, NBS Technical Note 1010 (Feb. 1979).
15. Abramowitz, M., and Stegun, I., Handbook of mathematical functions, NBS Applied Mathematics Series 55, p. 299.